Direct Kinetics and Product Measurement of Phenyl Radical + Ethylene

THE JOURNAL OF PHYSICAL CHEMISTRY A

pubs.acs.org/JPCA Article

Direct Kinetics and Product Measurement of Phenyl Radical + Ethylene

Te-Chun Chu, Zachary J. Buras, Brook Eyob, Mica C. Smith, Mengjie Liu, and William H. Green*

Cite This: J. Phys. Chem. A 2020, 124, 2352−2365 Read Online

ACCESS | Metrics & More | Article Recommendations | Supporting Information

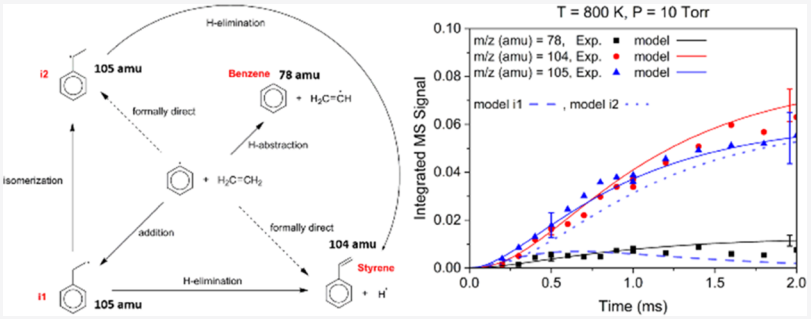

ABSTRACT: The phenyl + ethylene (C_6H_5 + C_2H_4) reaction network was explored experimentally and theoretically to understand the temperature dependence of the reaction kinetics and product distribution under various temperature and pressure conditions. The flash photolysis apparatus combining laser absorbance spectroscopy (LAS) and time-resolved molecular beam mass spectrometry (MBMS) was used to study reactions on the C_8H_9 potential energy surface (PES). In LAS experiments, 505.3 nm laser light selectively probed C_6H_5 decay, and we measured the total C_6H_5 consumption rate coefficients in the intermediate temperature region (400−800 K), which connects previous experiments performed in high-temperature (pyrolysis) and low-temperature (cavity-ring-down methods) regions. From the quantum chemistry calculations by Tokmakov and Lin using the G2M(RCC5)//B3LYP method, we constructed a kinetic model and estimated phenomenological pressure-dependent rate coefficients, $k(T, P)$, with the Arkane package in the reaction mechanism generator. The MBMS experiments, performed at 600−800 K and 10−50 Torr, revealed three major product peaks: m/z = 105 (adducts, mostly 2-phenylethyl radical, but also 1-phenylethyl radical, *ortho*-ethyl phenyl radical, and a spiro-fused ring radical), 104 (styrene, co-product with a H atom), and 78 (benzene, co-product with C_2H_3 radical). Product branching ratios were predicted by the model and validated by experiments for the first time. At 600 K and 10 Torr, the yield ratio of the H-abstraction reaction (forming benzene + C_2H_3) is measured to be 1.1% and the H-loss channel (styrene + H) has a 2.5% yield ratio. The model predicts 1.0% for H-abstraction and 2.3% for H-loss, which is within the experimental error bars. The branching ratio and formation of styrene increase at high temperature due to the favored formally direct channel (1.0% at 600 K and 10 Torr, 5.8% at 800 K and 10 Torr in the model prediction) and the faster β-scission reactions of C_8H_9 isomers. The importance of pressure dependence in kinetics is verified by the increase in the yield of the stabilized adduct from radical addition from 80.2% (800 K, 10 Torr) to 88.9% (800 K, 50 Torr), at the expense of styrene + H. The pressure-dependent model developed in this work is well validated by the LAS and MBMS measurements and gives a complete picture of the C_6H_5 + C_2H_4 reaction.

1. INTRODUCTION

In past decades, the formation of polycyclic aromatic hydrocarbons (PAHs) has attracted attention in astrochemical[1−4] and combustion[5−8] research. This chemistry is also important in processes for making coke, carbon black, and carbon nanotubes and in a variety of deposit formation mechanisms.[9−12] The simplest aromatic radical, phenyl radical (C_6H_5), reacts with unsaturated hydrocarbons and forms a second ring through radical cyclization. PAHs in astrochemistry have been correlated with the unidentified infrared (UIR) emission band ranging from 3 to 14 μm[13−16] and recognized as a carrier of the diffuse interstellar bands (DIBs) in the low-wavelength visible (400 nm) to the near-infrared (1200 nm).[14,17,18] Due to their abundant existence in some carbon-rich environments, PAHs are known to be important in the evolution of the interstellar medium (ISM).[19−21] While their existence is advantageous in the field of astronomy, PAHs as precursors to soot formation are normally undesired side products in chemical processing and combustion and

Received: December 13, 2019
Revised: February 27, 2020
Published: March 2, 2020

https://dx.doi.org/10.1021/acs.jpca.9b11543
J. Phys. Chem. A 2020, 124, 2352−2365

contribute to air pollution[11,22] and global warming.[23] In efforts to minimize the yield of PAHs, numerous potential energy surfaces (PESs) involving PAH initiation and propagation have been calculated and applied to mechanisms used in industrial chemical processes, and species like styrene are important in PAH formation.[24−27] To validate the theoretical works, kinetics measurements and product quantification under different conditions have been designed and performed.

As one of the simplest unsaturated hydrocarbons, ethylene (C_2H_4) and its reaction with C_6H_5 and products on the corresponding PES have been recognized as important in various fields. The radical addition product, 2-phenylethyl radical, has been used as a carbon-centered radical interacting with DNA to study the metabolic activation of hydrazine derivatives.[28−31] Another radical adduct formed through 2-phenylethyl radical isomerization is 1-phenylethyl radical, and it has been selected as a model species to react with various monomers to understand their reactivity toward the polystyrene radical.[32−35] In this reaction network, styrene can be generated through the well-skipping reaction from C_6H_5 + C_2H_4 and H-elimination from radical adducts.

To measure the kinetics of C_6H_5 + C_2H_4, Fahr et al. performed low-pressure pyrolysis experiments from 1000 to 1330 K and styrene was proposed as a reaction product.[36,37] However, in this experiment, a large fraction of the carbon was deposited on the reactor wall, which caused C_6H_5 loss and affected rate quantification. The cavity-ring-down (CRD) method was used by Yu and Lin[38,39] to measure total rate constants of C_6H_5 + C_2H_4 between 297 and 523 K; moreover, their multichannel RRKM analysis explained the discrepancy between the previous pyrolysis experiments and their CRD measurement. Zhang et al. investigated styrene formation with a crossed molecular beam setup under single-collision conditions.[40] The product styrene was found along with a H atom from a short-lived transient species after a collision between C_6H_5 and C_2H_4. The experiment also found the reaction phenyl + ethene → styrene + H to be exoergic by 25 ± 12 kJ/mol (6.0 ± 2.9 kcal/mol). Using improved quantum chemical methods at the G2M level of theory,[41] Tokmakov and Lin completed a detailed analysis on the C_6H_5 + C_2H_4 PES including hindered rotor calculations.[42] Rate constants of all elementary reactions were computed using the transition state theory (TST), and the calculated rate for the initial addition step agreed well with the previous pyrolysis and CRD experiments. RRKM/ME calculations were performed as well to get $k(T)$ at two different pressures. The energy released in styrene + H formation was calculated as 7.1 kcal/mol, consistent with the crossed molecular beam results. Product branching ratios were predicted at different T, P conditions; however, no experimental data was available at that time to provide direct validation. As suggested by Yu and Lin,[38] more experimental data on the product formation are needed to improve kinetic models.

In this work, time-resolved molecular beam mass spectrometry (MBMS) experiments of the C_6H_5 + C_2H_4 reaction are coupled with a pressure-dependent model derived from the complete molecular information reported by Tokmakov and Lin[42] to directly quantify product formation under a range of T, P (600−800 K, 10−50 Torr) conditions. Laser absorbance spectroscopy (LAS) experiments are conducted in the same apparatus to measure the total rate coefficients of C_6H_5 + C_2H_4 from 400 to 800 K.

2. EXPERIMENTAL METHODS

The experimental apparatus used in this work has been described in previous publications.[43−46] Two types of experiments were performed in this apparatus. First, LAS was used to measure phenyl radical (C_6H_5) consumption rates; second, time-resolved MBMS was used to evaluate the product formation and branching ratios.

All experiments were performed in a custom quartz flow reactor (1.6 cm inner diameter in the center section where the measurement takes place) sampled to a high vacuum chamber with a time-of-flight mass spectrometer (TOF-MS); the TOF-MS has the mass resolution, $m/\Delta m$, ∼400, which can easily distinguish chemical species with the mass-to-charge ratio (m/z) values separated by 1 amu.[45] Gases were well-mixed before flowing into the reactor, which is pumped by a Roots blower. Pressure in the reactor was controlled between 4 and 50 Torr by throttling a butterfly valve at the reactor outlet. The reactor was wrapped with a nichrome ribbon wire to heat up the gas to desired temperatures (room temperature to 800 K) measured by two thermocouples located inside the reactor. Axial temperature profiles of the gas were measured in the previous work,[45] and temperatures with uncertainty for each experimental condition are reported in this work. For absorbance experiments, the temperature was evaluated from the region where the Herriott cell and photolysis overlap; for MBMS experiments, only the 5 cm section on the inlet side of the sampling pinhole was chosen to report average temperatures with uncertainties, corresponding to the distance traveled on the short reaction time scale (up to 2 ms) in this work.

A collimated 266 nm laser beam (fourth harmonic frequency of an Nd:YAG laser) was used to photolyze the radical precursor. The repetition rate was set at 1 Hz, except for a few control experiments at 2 Hz, and the total gas flow rate was controlled to maintain one flash-per-refresh (FPR) conditions. Before the laser beam entered the reactor, an adjustable iris was placed in the beam path to control the beam diameter. It was clipped from 1.8 to 1.5 cm, which is slightly smaller than the reactor's inner diameter, providing two main advantages: 1. Clipping the edges of the beam can decrease inhomogeneities in the radical concentration. 2. No direct contact was made between the reactor inner wall and the laser beam, but the beam was carefully aligned to minimize the gap between the irradiated volume and the reactor wall. This reduced the risetime of the MS signal after the photolysis flash, allowing us to measure product distribution with less interference from secondary reactions. In previous MBMS experiments,[46] we observed significant conversion of phenyl radical to benzene, but that was much less of a problem in the present work possibly because the improved alignment and faster risetime reduced wall reactions.

The wavelength of the probe laser in LAS experiments was 505.3 nm, which is close to the reported C_6H_5 low-lying electronic transition at 504.8 nm.[38,47] At this wavelength, the main product radicals formed in the experiments (the phenylethyl radicals and vinyl radicals) are not expected to absorb and interfere with the kinetics evaluation.[39,48] In MBMS experiments, the photoionization laser beam at 118.2 nm (10.5 eV, ninth harmonic frequency of an Nd:YAG laser) intersected with the molecular beam produced by sampling from a 275 μm diameter pinhole in the center of the reactor. The ionized species were accelerated, focused, and guided to

https://dx.doi.org/10.1021/acs.jpca.9b11543
J. Phys. Chem. A 2020, 124, 2352−2365

the KORE TOF-MS detector (ETP electron multiplier, model AF824).

Iodobenzene (C_6H_5I; Sigma-Aldrich, 98%) was used as the photolytic precursor of phenyl radical (C_6H_5). To remove oxygen and impurities, several freeze-pump-thaw cycles were performed on C_6H_5I in an air-tight bubbler.[46] Due to the high reactivity between C_6H_5 and O_2, a strong 505 nm absorbance signal from the product phenylperoxy (C_6H_5OO) can be observed when ≥100 ppm of O_2 remains in the bubbler.[49,50] Before each experimental condition, absorbance traces of C_6H_5 without C_2H_4 were taken to ensure that O_2 is eliminated. The co-product of photolysis from C_6H_5I, I atom, has the same initial concentration as C_6H_5; therefore, the 1315 nm transition of the I atom was probed to determine the initial C_6H_5 concentration.[46] Helium (He) was the bath gas for all experiments with UHP grade purity (≥99.999%) obtained from Airgas. Ethylene (C_2H_4) had ≥99.5% purity (CP grade) and was purchased from Airgas.

3. THEORETICAL METHODS

3.1. Potential Energy Surface and Kinetics Calculation. The C_8H_9 potential energy surface was calculated by Tokmakov and Lin using G2M(RCC5)//B3LYP.[42] Three pairs of bimolecular products were reported: phenyl + ethylene, vinyl + benzene, and H + styrene, along with five adducts on the PES, which is depicted in Figure 1. Four other

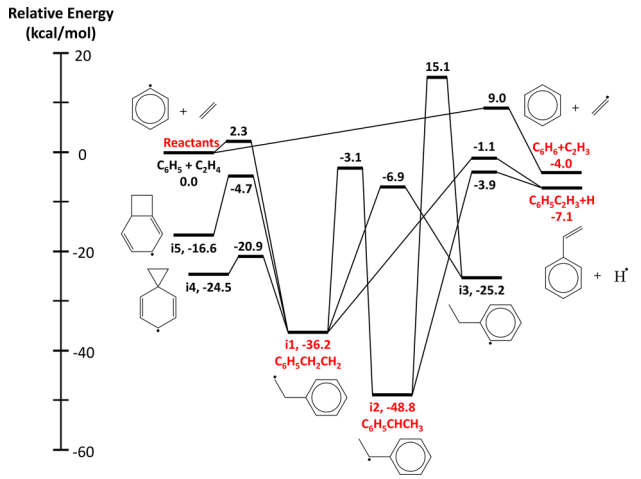

Figure 1. Phenyl radical + ethylene (C_8H_9) potential energy surface with important species and pathways calculated by Tokmakov and Lin using G2M(RCC5)//B3LYP/6-311++G(d,p). Dominant species at the conditions of this work are labeled in red.

C_8H_9 isomers reported by Tokmakov and Lin[42] (i6−i9) have less significance in the conditions of this work; however, the corresponding reactions are included in our mechanism and presented in the expanded PES Figure S1. Other reactions were considered by Tokmakov and Lin;[42] however, those reactions were not included in their reported PES since the reaction barriers were too high. In previous works, total rate coefficients evaluated from the PES were validated by Fahr et al.'s experimental data (1000−1330 K)[36,37] and Yu and Lin's cavity-ring down experiments,[38,39] despite small systematic errors (1−2 kcal/mol) in the enthalpies and barriers for radical additions producing Π-radicals with a large degree of electron delocalization at the level of theory.[42] Tokmakov and Lin's prediction on product branching ratios had no experimental data to validate. The predicted rate coefficients and time-dependent composition of the species on the C_8H_9 PES were reported[42] at some T and P, but not at the conditions of our experiments.

In this work, we used Arkane,[51] a program in the open-source Reaction Mechanism Generator (RMG)[52] software package, to compute both high pressure and phenomenological pressure-dependent rate coefficients, $k_\infty(T)$ and $k(T, P)$, from the molecular information provided by Tokmakov and Lin with some modest extensions. At the high-pressure limit, canonical transition state theory (TST) was used with the rigid-rotor harmonic oscillator (RRHO) approximation to evaluate rate coefficients. The one-dimensional (1D) hindered rotor treatment was applied to replace the frequencies in square brackets in Tokmakov and Lin's Supporting Information,[42] which indicated internal rotations with low-energy barriers. 1D-asymmetric Eckart correction was chosen as the tunneling model. High-pressure limit rate coefficients of all elementary steps on the PES are reported in the Supporting Information.

When temperature increases, pressure decreases, or molecular size decreases, significant falloff or chemical activation effects may take place, and the pressure dependence of the kinetics should be considered. In our experiments, pressure ranged between 4 and 50 Torr, so many reactions were not in the high-pressure limit. Therefore, phenomenological pressure-dependent rate coefficients, $k(T, P)$, were computed with Arkane and used in the model to compare with experimental results. Using the modified strong collision approximation, $k(T, P)$ were fitted into the Chebyshev format by applying RRKM/ME from the ab initio data provided by Tokmakov and Lin.[51] Lennard-Jones parameters between He and the C_8H_9 adducts (ϵ/cm^{-1}, σ/Å = 342, 6.83) were estimated by the Joback method[53] implemented in RMG. Collisional energy-transfer parameters ($\alpha(T)$ = 424*(T/300 K)$^{0.62}$ cm^{-1}) were taken from Mebel et al.[54] for argon bath gas and scaled down for helium bath gas using the calculations of Jasper et al.[55]

The pressure-dependent forward rate coefficients on the C_8H_9 PES are from our master equation calculations based on Tokmakov and Lin's ab initio calculations at the stationary points. To ensure thermodynamic consistency, all of the reverse rate coefficients in the kinetic model are computed from the forward rate coefficients and equilibrium constants computed using the NASA polynomials for each species given in the Supporting Information. The database available in RMG has ∼40 libraries, which store thermochemistry properties from the literature or ab initio quantum chemistry calculation. Among these, the Narayanaswamy library[56] focuses on aromatics formation and contains accurate experimental data along with G3MP2//B3 calculations, so it was used to estimate thermochemical properties of dominant species (C_6H_5, C_2H_4, C_6H_6, C_2H_3, $C_6H_5C_2H_3$, i1) on the PES in Figure 1, except for the H atom, which was taken from primaryThermoLibrary.[52] The thermochemistry of 1-phenylethyl radical (species i2 in Figure 1) was found to sensitively affect the predicted adduct isomerization and styrene formation rates at some reaction conditions; however, its thermochemical properties were not available in any libraries. Therefore, ab initio calculation of 1-phenylethyl radical was performed at the CCSD(T)-F12/cc-pVTZ-F12//wB97x-D3/def2-TZVP level of theory with 1D hindered rotors using MOLPRO 2015[57−67] and Q-Chem 4.4.0.[68] That species' enthalpy, entropy, and heat capacity were

https://dx.doi.org/10.1021/acs.jpca.9b11543
J. Phys. Chem. A 2020, 124, 2352−2365

Scheme 1. Overall Approach to Predict Species Concentrations and Convert Them into MBMS Signals for Comparison With Experimental Data

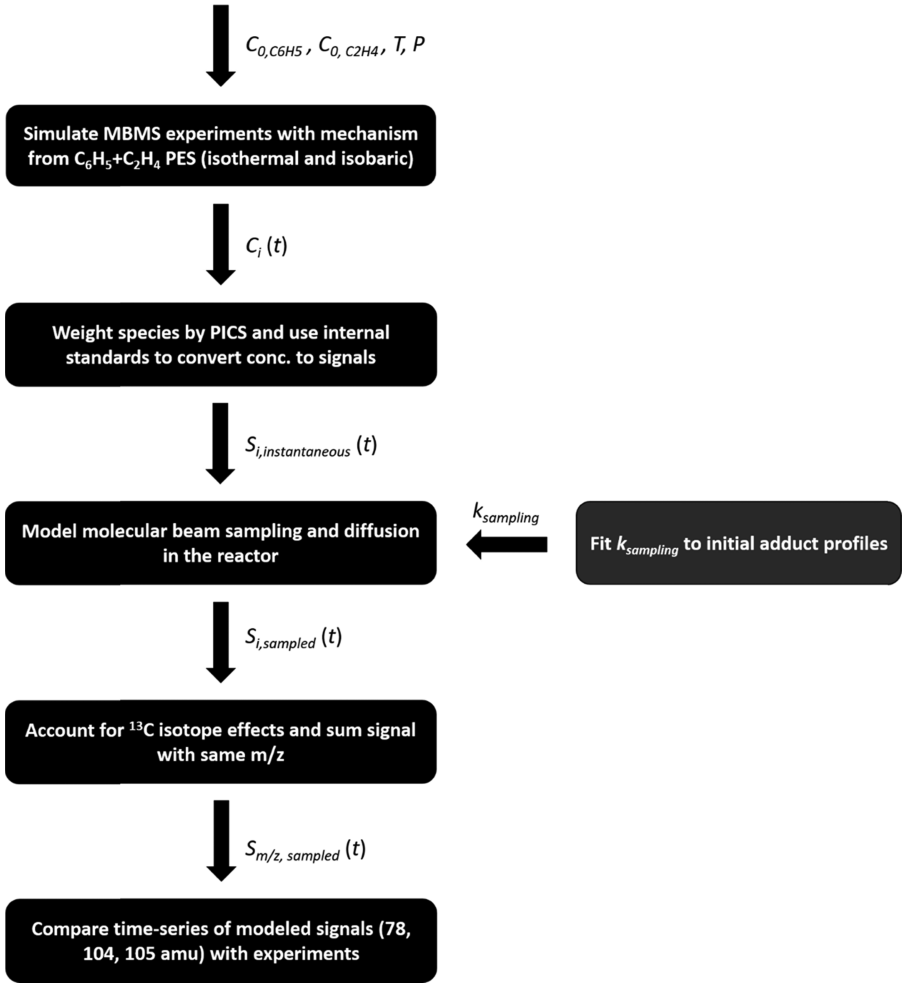

then evaluated in Arkane and used in the mechanism. For the rest of the species containing aromatic rings, RMG was used to estimate their thermochemistry properties based on two improved algorithms: similarity matching and bicyclic decomposition, which extended the basic group additivity method.[69] Although the accuracy of the prediction is not as great as ab initio calculations or library values, a sensitivity analysis showed that the energy of those species have insignificant effect on the product formation, which will be thoroughly discussed in the Results and Discussion section. The full pressure-dependent mechanism including kinetics and species thermochemistry in the Chemkin format and the corresponding species dictionary with RMG-style adjacency lists of the species in the model are included in the Supporting Information. Although the Chebyshev format is recommended here to express pressure-dependent kinetics, the Plog format kinetics are also provided in the Supporting Information. Sensitivity analysis was performed using Arkane (sensitivity of reaction rate constants to species energy) and RMG (sensitivity of species concentration to reaction rate constants and species enthalpy), and rate of production (ROP) analysis was done using Chemical Workbench.[70]

3.2. Modeling MBMS Experiments. The approach for modeling the MBMS experiments in this study is similar to what was described in Buras et al.'s work on phenyl radical + propene.[46] The main difference is the time scale studied; a short time scale up to 2 ms was used in this work to focus on the primary chemistry and minimize secondary reactions (product formation, which is not directly from C_6H_5 + C_2H_4) and side reactions (reactions not on the C_6H_5 + C_2H_4 PES). Scheme 1 shows the procedure for modeling MBMS experiments and converting predicted species concentrations obtained in the model into predicted signals, which can be compared with MBMS experimental data.

In the MBMS experiments, three main product peaks were observed: m/z = 105 (adducts, i1 and i2), m/z = 104 (H-loss product, styrene), and m/z = 78 (H-abstraction product, benzene). To validate the combined mechanism generated with pressure-dependent kinetics and species thermochemistry properties, simulations were performed with an isothermal and isobaric batch reactor at temperature and pressure conditions from each of the MBMS experiments. With the initial phenyl radical concentration ($C_{C_6H_5,0}$) taken from the I atom laser measurement, the simulation predicted time-dependent concentrations (C_i) of each species on the PES. Each product species was then weighted by its photoionization cross section (PICS, σ) at 10.5 eV. For stable products, PICS were taken from previously reported values: $\sigma_{10.5\ eV,\ benzene}$ = 31.8 ± 6.4 Megabarns (Mb),[71] $\sigma_{10.5\ eV,\ styrene}$ = 43.9 ± 4.4 Mb.[72] For radical products, some assumptions based on the literature were needed to estimate PICS as follows. Due to a

https://dx.doi.org/10.1021/acs.jpca.9b11543
J. Phys. Chem. A 2020, 124, 2352−2365

correspondingly lower occupancy of the highest occupied molecular orbital (HOMO) from which the electron is ejected in radicals, a decrease in PICS by a factor of 2−4 compared to their closed-shell analogues can be expected.[73] However, aromatic resonance-stabilized radicals (RSRs) may have PICS similar to their closed-shell counterparts, for example, the PICS of benzyl radical $\sigma_{10.5\ eV,\ benzyl}$ = 25.5 Mb[74] at 10.5 eV is close to that of the related closed-shell structure, toluene (32.0 Mb[72]). Therefore, the PICS is estimated as 10 ± 5 Mb for the nonresonant 2-phenylethyl radical (i1) and 30 ± 6 Mb for the resonance-stabilized 1-phenylethyl radical (i2, RSR) in this work, given the PICS of 32.1 Mb[72] for ethylbenzene, the closed-shell analogue of i1 and i2. The above PICS is used with a response factor obtained from internal standards (present in the reactor at ∼1 × 10^{11} molecule/cm^{-3}) to calculate signals from the predicted time-dependent concentration for species i

$$S_{i,\mathrm{model}} = R(\mathrm{int.\ std.})\sigma_{10.5\ \mathrm{eV},i}C_i,\ \text{where } R(\mathrm{int.\ std.}) = \frac{S_{\mathrm{int.std.}}}{\sigma_{10.5\ \mathrm{eV,int.std.}}\ C_{\mathrm{int.std}}} \quad (1)$$

To account for the transport effects in the reactor and molecular beam sampling, a simple model with the first-order rate constant (k_{sampling}) was utilized, which was adapted from Baeza-Romero et al.[75] by Buras et al.[46] In this work, k_{sampling} was fitted to the measured risetime of the m/z = 105 signal (initial adduct). The fitted k_{sampling} is validated by the normalized signals of I atom at m/z = 127; Figure S2 presents an example at 700 K, 10 Torr. Finally, before summing all modeled species signals of the same m/z and comparing with the experiments, the impact of ^{13}C isotopes was assumed to contribute 1.1% x number of carbon atoms for each of the product. This is especially important for m/z = 105, where the adduct signal is overlapped by the ^{13}C satellite of styrene.

4. RESULTS AND DISCUSSION

4.1. Overall $k(T)$ of C_6H_5 + C_2H_4 Measured by 505.3 nm Absorbance. In absorbance experiments, 505.3 nm absorbance was used to measure the total consumption rate coefficient, $k_{\mathrm{total}}(T)$, of C_6H_5. The absorption cross section for C_6H_5 was measured at 504.8 nm by Tonokura et al.[47] In our experiments, greater absorbance signals at 505.3 nm were observed compared to that measured at 504.8 nm, and other radicals formed on the C_8H_9 PES, i.e., 1-phenylethyl, 2-phenylethyl, and vinyl radicals, were not expected to have observable absorbance at this wavelength. At the high-pressure limit, $k_{\mathrm{total}}(T)$ is composed of two channels: radical addition (forming i1) and H-abstraction (forming C_6H_6 + C_2H_3). In Figure 3, the predicted kinetics from Tokmakov and Lin shows that the H-abstraction channel has negligible rates at low temperatures (<1000 K) compared to the radical addition channel. From the barrier heights calculated and reported in Figure 1, the H-abstraction barrier (9.0 kcal/mol) is much higher than the radical addition barrier (2.3 kcal/mol), so the much slower H-abstraction kinetics and minor product branching of C_6H_6 are expected.

Before each absorbance experiment, background absorbance signals were recorded by flowing pure helium or helium + ethene with the same photolysis laser fluence as the kinetics experiments. Some nonzero background signals were observed, which may come from the slightly shifted probe laser beam caused by scattered photolysis light reflected by the Herriott cell optics.[46] Therefore, background subtraction was performed on all absorbance traces. The background-corrected signal traces were then fit to an exponential decay expression assuming pseudo-first-order kinetics

$$A(t)/A_0 = a + (1 - a)e^{-k't},\ \text{where } k' = k_{\mathrm{total}}[C_2H_4] + k_{\mathrm{wall}} \quad (2)$$

Because of noise, imperfect background subtraction, and artifacts from AC-coupled detection electronics, a vertical shift factor (a) was used to account for the baseline offsets, which was normally within 10% and never exceeding 20% of the peak signal. Except for the gas-phase reaction of C_6H_5 + C_2H_4 measured, other reactions like wall reaction, self-recombination, reaction with impurities like oxygen, and reaction with the precursor would lead to C_6H_5 consumption and change in absorbance signals, and all of those reactions are collected in the term k_{wall}. By increasing C_2H_4 concentration at the same T, P condition, a faster decay of C_6H_5 was observed with larger k' fitted, which is shown in Figure 2. With at least five points on the plot of [C_2H_4] versus k', k_{total} (slope) and k_{wall} (y-intercept) were acquired from the fitted straight line.

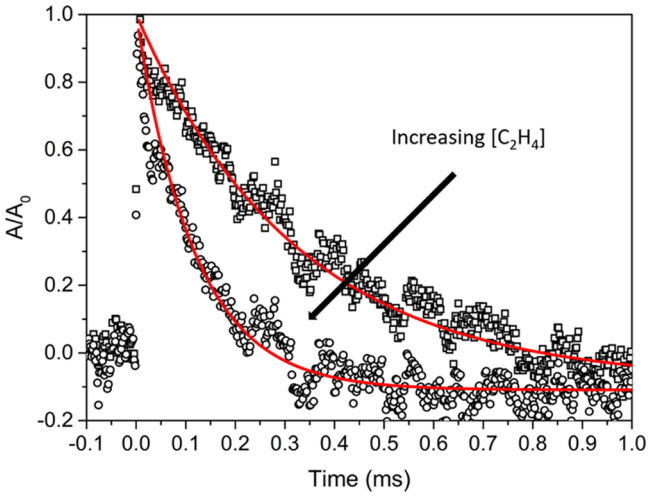

Figure 2. Representative 505.3 nm absorbance decays measured (markers) at 700 K, 10 Torr. Lines are exponential fits. Data plotted are the average value of every 40 data points.

Table 1 summarizes the conditions and results of absorbance experiments from 400 to 800 K. Temperatures were measured for the region where the Herriott cell and the photolysis laser overlap, which was 20 cm long with 20% uncertainty. All experiments were performed at 10 Torr, except for Experiment 6 at 50 Torr. Experiments 7 and 8 were control experiments to test the effect of changing photolysis laser energy (20 to 35 mJ/pulse) and flash-per-refresh (FPR, 1 to 2). The rate coefficients measured in the control experiments fall within the uncertainty range of those measured at the standard conditions at 800 K (Experiment 5), which indicates that changing pressure, laser energy, and FPR have a negligible effect on the measured disappearance of C_6H_5 due to C_6H_5 + C_2H_4. The initial concentration of C_6H_5 was determined by single-pass IR absorbance of the I atom (in the $^2P_{1/2} \leftarrow {}^2P_{3/2}$ transition[76]) generated simultaneously with C_6H_5 after the photolysis pulse; this method was used in our previous works.[46,77] All experiments were carried out for at least five different concentrations of C_2H_4. In the Supporting Information, plots

https://dx.doi.org/10.1021/acs.jpca.9b11543
J. Phys. Chem. A 2020, 124, 2352−2365

Table 1. Summary of Absorbance Experiments at 505.3 nm Measuring k_{total} of C_6H_5 + C_2H_4[a]

exp. #	nominal T (K)	measured T (K)	P (Torr)	photolysis energy (mJ/pulse)	$[C_6H_5]_0$ (10^{12} cm^{-3})	$[C_2H_4]$ range (10^{15} cm^{-3})	number of traces	k_{total} (10^{-14} cm^3 s^{-1})	k_{wall} (s^{-1})	range of a[b]
1	400	400.0 ± 1.5	10	20	2.2 ± 0.7	42.9 ± 8.6−150 ± 30	6	1.14 ± 0.23	710 ± 142	−0.08 to 0.06
2	500	495.1 ± 2.6	10	20	2.7 ± 0.9	32.2 ± 6.4−129 ± 26	7	2.08 ± 0.42	729 ± 146	−0.05 to 0.08
3	600	592.1 ± 4.1	10	20	2.9 ± 0.9	21.5 ± 4.3−7.51 ± 15.0	5	5.05 ± 1.02	219 ± 44	0.05 to 0.12
4	700	696.2 ± 3.7	10	20	3.1 ± 1.0	15.9 ± 3.2−55.7 ± 11.1	5	9.20 ± 2.84	542 ± 108	−0.22 to −0.14
5	800	793.8 ± 7.0	10	20	2.1 ± 0.9	17.7 ± 3.5−30.6 ± 6.1	5	11.2 ± 2.2	789 ± 158	−0.02 to 0.15
6	800	787.3 ± 7.1	50	20	2.1 ± 1.0	11.3 ± 2.3−27.4 ± 5.5	6	10.5 ± 2.1	593 ± 119	0.05 to 0.16
7	800	793.8 ± 7.0	10	35	3.9 ± 1.6	14.5 ± 2.9−30.6 ± 6.1	6	11.9 ± 2.4	174 ± 35	0.02 to 0.04
8[c]	800	793.8 ± 7.0	10	20	2.2 ± 1.0	17.7 ± 3.5−30.6 ± 6.1	5	12.8 ± 2.6	871 ± 174	0.03 to 0.08

[a]All experiments were performed at a precursor concentration of 6.5 × 10^{13} cm^{-3} (upper limit assuming that He exiting the bubbler is saturated with C_6H_5I at its room temperature and using a vapor pressure of 0.92 Torr for C_6H_5I[78]). [b]Vertical shift in fits to normalized absorbance traces. [c]Changing the repetition rate of the photolysis laser from 1 to 2 Hz.

of k' versus $[C_2H_4]$ (Figure S3) and all k' values in Experiment 1−8 are provided. The wall loss rate k_{wall} accounts for a relatively small portion in the decay of C_6H_5, except for experiment 8 where k_{wall} is larger than 1000 s^{-1} possibly due to the misaligned photolysis laser that generates radicals on the wall or reaction products from the prior flash since experiment 8 was operated with double flash-per-refresh; however, the contribution of k_{total} was still more than a factor of three greater than k_{wall}.

To compare with previous experiments on C_6H_5 + C_2H_4 kinetics, Figure 3 plots the measurements of Fahr et al. (1000−1300 K, pyrolysis/mass spectrometer measuring styrene formation)[36,37] and Yu et al. (297−523 K, flash photolysis/cavity-ring-down (CRD))[38] along with the results from this work. The measured $k_{total}(T)$ here is in the intermediate temperature range (400−800 K). In Fahr et al.'s experiments, fall-off kinetics happened at high-temperature conditions, and the measurement was rationalized by Yu et al.[38] using RRKM analysis. Combining the three experimental datasets provides a complete picture of the temperature behavior from room temperature to 1300 K. The experimental data agree with the predicted $k_{total}(T)$ from ab initio calculations allowing for a 1 kcal/mol uncertainty in barriers. Therefore, $k_{total}(T) = k_{R\text{-addition}} + k_{H\text{-abstraction}} = (4.41 \times 10^5)T^{1.96}\exp(-971/T) + (9.45 \times 10^{-3})T^{4.47}\exp(-2250/T)$ [cm^3/mol s] reported by Tokmakov and Lin[42] is recommended for future kinetics related works. Within 400−800 K at 10 Torr, the Arrhenius expression $k_{total}(T) = (3.85 \times 10^4)T^{2.30}\exp(-695.9/T)$ [cm^3/mol s] is obtained based on our experimental measurement.

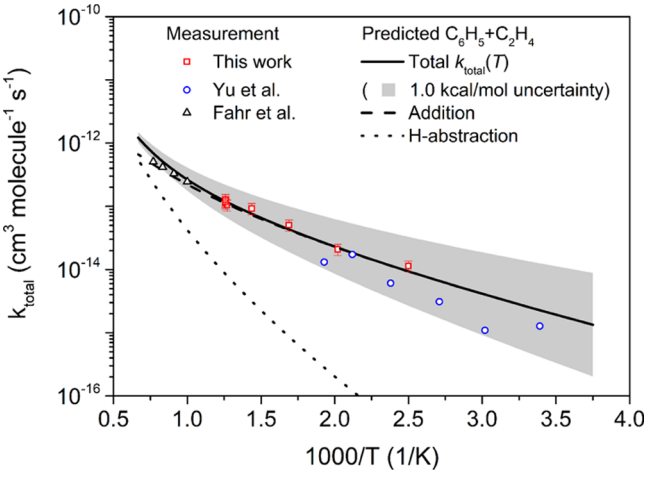

Figure 3. Total C_6H_5 consumption rate coefficients measured in this work (400−800 K) and the predicted temperature dependence from ab initio calculations of Tokmakov and Lin. Previous experimental measurements at different temperature ranges from Fahr et al. (1000−1300 K) and Yu and Lin (297−523 K) are also shown.

4.2. Products Measured by MBMS Experiments. For the C_6H_5 + C_2H_4 system, three product peaks were observed in the MBMS experiments: m/z = 105 (the initial adduct i1 and its isomers plus ^{13}C satellite of m/z = 104), m/z = 104 (H-loss product, styrene), and m/z = 78 (H-abstraction product, benzene). Figure 4 shows representative time-resolved mass spectra after the subtraction of prephotolysis background signals. These background signals mainly result from C_6H_5I with some impurity peaks and fragmentation; a representative background mass spectrum is shown in Figure S4. In addition

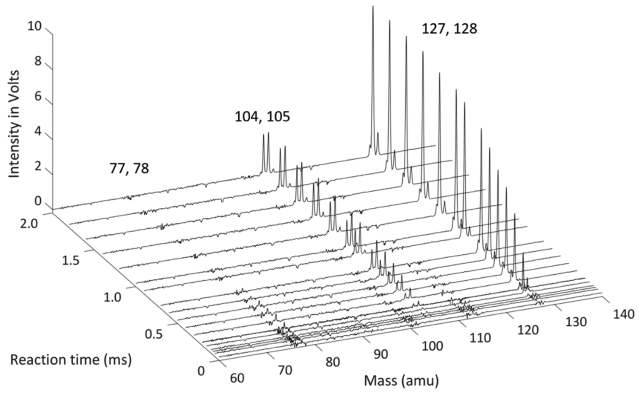

Figure 4. Representative background-subtracted, time-resolved mass spectra, measured at 800 K and 10 Torr. The large peak at 127 amu is from I atom formed by photolyzing phenyl iodide.

https://dx.doi.org/10.1021/acs.jpca.9b11543
J. Phys. Chem. A 2020, 124, 2352−2365

Table 2. Conditions of MBMS Experiments Measuring Products of C_6H_5 + C_2H_4[a]

exp. #	nominal T (K)	real T (K)	P (Torr)	photolysis energy (mJ/pulse)	$[C_6H_5]_0$ (10^{12} cm^{-3})	$[C_2H_4]$ (10^{15} cm^{-3})	$k_{sampling}$ (s^{-1})	$t_{90\%}$ (ms)[b]
9	600	607.4 ± 0.6	10	20	2.9 ± 0.9	59.0 ± 11.8	3500	1.13
10	700	711.1 ± 0.7	10	20	3.0 ± 1.0	24.1 ± 4.8	3500	1.37
11	700	711.1 ± 0.7	10	20	3.0 ± 1.0	34.9 ± 7.0	3500	0.90
12	800	795.9 ± 1.0	10	20	2.2 ± 1.0	16.1 ± 3.2	3500	0.98
13	800	795.9 ± 1.0	10	20	2.2 ± 1.0	26.8 ± 5.4	3500	0.74
14	800	795.9 ± 1.0	10	30	2.2 ± 1.0	26.8 ± 5.4	2500	0.84
15	800	786.8 ± 1.3	50	20	2.0 ± 1.0	16.1 ± 3.2	3500	0.82
16	800	786.8 ± 1.3	50	20	2.0 ± 1.0	26.8 ± 5.4	3500	0.60

[a]All experiments were performed at a precursor concentration of 6.5 × 10^{13} cm^{-3} (upper limit assuming that He exiting the bubbler is saturated with C_6H_5I at its room temperature and using a vapor pressure of 0.92 Torr for C_6H_5I[78]). [b]Time at which 90% of phenyl radicals has been consumed, obtained from the absorbance traces at the same reaction conditions using eq 2.

to the three product peaks of greatest interest, signals from phenyl radical (m/z = 77), I atom (m/z = 127), HI (m/z = 128), and hydrocarbon impurities (m/z = 92 from the calibration mixture, 112 from the C_6H_5I precursor) can be observed. The signal at m/z = 154 corresponding to biphenyl ($C_{12}H_{10}$) is negligible in the mass spectra, suggesting that the reactions C_6H_5 + C_6H_5 → $C_{12}H_{10}$ and C_6H_5 + C_6H_5I → $C_{12}H_{10}$ + I are not important in this study. For the phenyl radical, the integrated signal reaches the maximum 0.3 to 0.5 ms after the photolysis pulse instead of t = 0 due to $k_{sampling}$ in each experiment. Compared to the absorbance experiments, a phenyl radical in the MBMS experiments has similar decay time; however, the nonideal time resolution of the MBMS experiments and the small PICS of phenyl radical made it difficult to evaluate the C_6H_5 + C_2H_4 total rate coefficients this way; LAS provides a much better way to determine k_{total}. The impurities mainly exist in ethylene (up to 1000 ppm of other hydrocarbons may be expected according to the stated purity) and the phenyl iodide precursor; however, no clear positive time dependence is observed for those impurities, so we conclude that the reaction of C_6H_5 + C_2H_4 is not affected. In addition to the impurities, the signal intensities of the calibration mixture have some fluctuation, which causes small peaks at those m/z values in the background-subtracted mass spectra in Figure 4. Vinyl radical, the co-product with benzene from the H-abstraction pathway, was observed at m/z = 27, but its small PICS made quantitative analysis impractical. The approach described in Section 3.2 was used to predict time-dependent product distributions. Experimental conditions are summarized in Table 2.

To minimize recombination and other side reactions but also ensure that the reaction time scale was longer than the sampling time scale, the concentration of C_2H_4 was controlled to achieve a reaction time of 1.5−2.0 ms. Similar to the absorbance experiments, the real temperature was determined by averaging over temperature measurements at different points in the reactor, in this case averaged over the 5 cm length on the upstream side of the center pinhole, which corresponds to the MBMS sampling region during the time after the flash. The pressure was 10 Torr for all experiments, except for experiments 15 and 16, which were performed at 50 Torr to understand the pressure dependence of product formation.

The value of $k_{sampling}$ was consistent (3500 s^{-1}) over the range of temperatures and pressures operated in most of the MBMS experiments. In experiment 14, the high photolysis energy or a shifted laser alignment may have caused an inhomogeneous concentration of the phenyl radical after the photolysis pulse and more diffusion, leading to a slightly slower sampling risetime of the MBMS signals ($k_{sampling}$ = 2500 s^{-1}). From previous experiments, the upper limit for time taken for transport via supersonic expansion to the ionization region due to effusive and supersonic sampling has been determined to be 100 μs.[75,79] The measured sampling time constant is slower than this, due to the time required to diffuse from the photolyzed region to the pinhole. In the present work, the sampling rate $k_{sampling}$ is higher than previous experiments[46] in the same apparatus (for which $k_{sampling}$ = 80−2000 s^{-1}) possibly because the photolysis laser beam was better aligned inside the reactor. With faster $k_{sampling}$, signals on a shorter time scale become observable and enable the quantification of the initial product distribution, even if they have sub-millisecond lifetimes.

Figure 5 shows time profiles of measured product peaks in MBMS experiments and the model prediction for experiments 9 (600 K, 10 Torr), 10 (700 K, 10 Torr), 12 (800 K, 10 Torr), and 15 (800 K, 50 Torr) up to ∼2 ms reaction time; other control experiments to test the effect of changing C_2H_4 concentration (reaction time ∼1.5 ms) and photolysis energy (20−30 mJ/pulse) are shown in the Supporting Information. In Figure 5, the model predictions are plotted with the MBMS experimental data, and uncertainty ranges of the model predictions due to uncertainties in PICS are shown as error bars. Due to the estimated PICS of radical species, large uncertainties can be found in the model prediction of m/z = 105 signals. To ensure that 2 ms was a reasonable time scale for C_6H_5 decay, absorbance traces at the same conditions were measured. The traces plotted in Figure 5, which are the average value of every 20 data points, and $t_{90\%}$ in Table 2 show that the C_6H_5 absorbance decays to less than 10% of its initial value within 2 ms, which indicates that the C_2H_4 concentration was sufficient. Detailed comparison of mass spectra and laser absorbance traces show the rate of product formation matches the rate of phenyl decay, though some noise can be observed in the traces. When we quantified the kinetics from the absorbance data described in Section 4.1, at least five C_2H_4 concentrations were used at a single T, P condition to minimize noise.

At 600 K, the experiment showed that the signal at m/z = 105 is dominant at early times due to the depletion of C_6H_5, while signals at m/z = 104 and 78 were very small. The modeled curve successfully predicts this behavior and attributes the adduct signals mostly to i1. This result suggests that once C_6H_5 + C_2H_4 crosses the radical addition barrier (2.3 kcal/mol) as seen in Figure 1, most of the addition products are thermalized to i1. When the temperature is increased to 700 K, the formation of styrene started to appear along with a

https://dx.doi.org/10.1021/acs.jpca.9b11543
J. Phys. Chem. A 2020, 124, 2352−2365

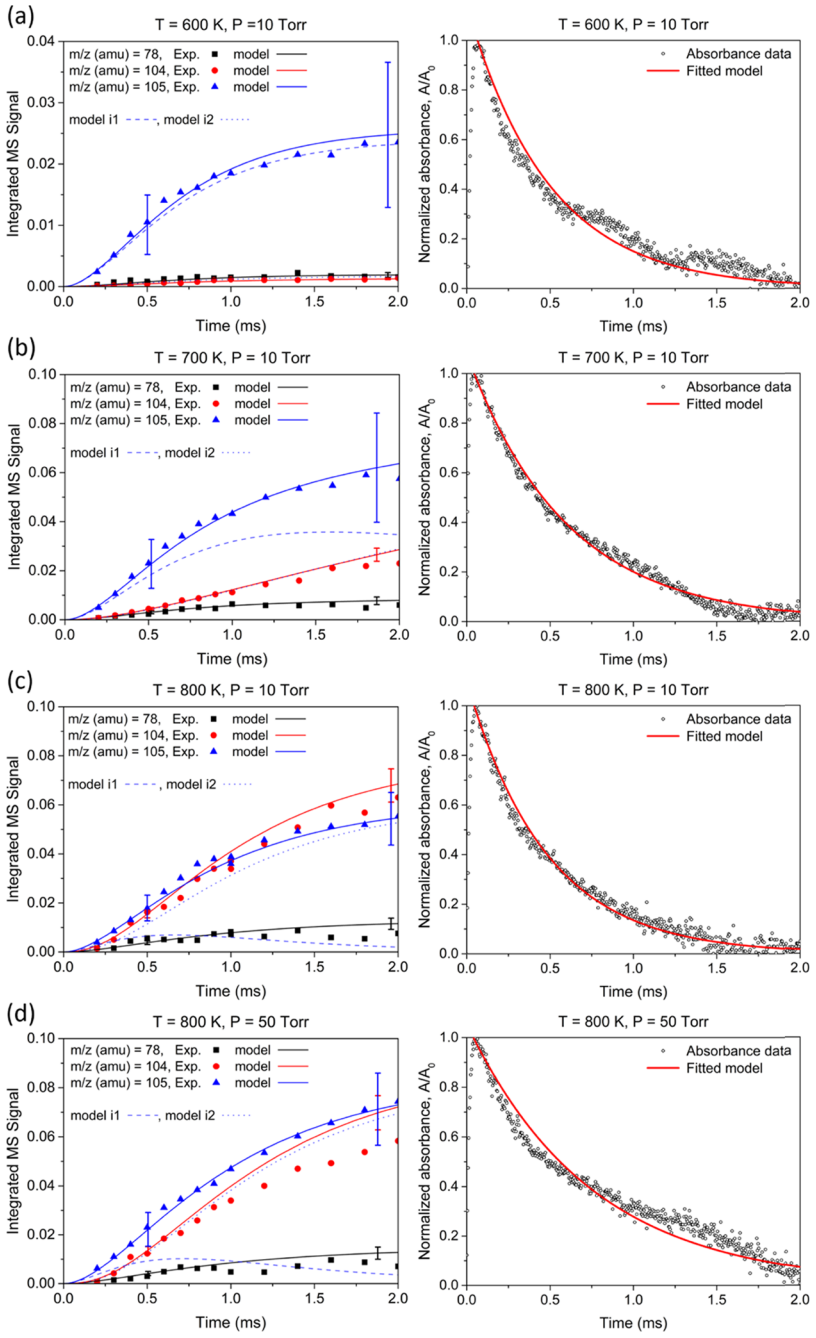

Figure 5. Experimental time profiles of primary product peaks measured by MBMS experiments and reactant (phenyl) decay measured by laser absorption. (symbols) The solid curves are the model predictions using PICS assumed in the text. Uncertainty ranges of the model predictions due to uncertainties in PICS are shown as error bars. Conditions: (a) 600 K, 10 Torr, $[C_2H_4]$ = 59.0 × 10^{15} molecule/cm^{-3}, (b) 700 K, 10 Torr, $[C_2H_4]$ = 24.1 × 10^{15} molecule/cm^{-3}, (c) 800 K, 10 Torr, $[C_2H_4]$ = 16.1 × 10^{15} molecule/cm^{-3}, (d) 800 K, 50 Torr, $[C_2H_4]$ = 16.1 × 10^{15} molecule/cm^{-3}. Experiments cannot distinguish i1 and i2, but the predicted signals of i1 and i2 from the model are shown as dashed lines. At 600 K, i1 dominates over the time scale measured; at 700 K, i1 is produced rapidly, while i2 increases slowly (almost overlapping with the styrene model line) and becomes similar to i1 at 2 ms; at 800 K, i2 dominates over i1 after 0.5 ms.

slight increase in benzene formation. The model again captures the product distribution from t = 0−2.0 ms and predicts that the formation of i2 increases gradually, whereas the formation of i1 reaches a plateau after 1.0 ms. In Figure 5b, the formation of styrene and i2 is predicted to occur on a similar time scale, such that the concentration of styrene and i2 is nearly the same at any given condition considering their PICS are close. This can be explained by their similar barrier heights (35.1 kcal/mol for styrene versus 33.1 kcal/mol for i2), which will be discussed more in the next section. At 800 K (Figure 5c,d), the highest temperature in this work, the signals of styrene were comparable to the sum of adduct signals dominated by i2. However, the benzene signals are still limited because the H-abstraction barrier is much higher than the radical-addition barrier, see Figure 3.

Unlike $k_{total}(T)$, which is pressure-independent, the product distributions and branching ratios are affected by pressure. From the analysis by Wong et al.,[80] for species on the C_8H_9

https://dx.doi.org/10.1021/acs.jpca.9b11543
J. Phys. Chem. A 2020, 124, 2352−2365

PES at 800 K, the switchover pressure (the pressure below which pressure dependence should not be neglected) falls within 0.01−0.1 atm (7.6−76 Torr). Therefore, increasing pressure from 10 to 50 Torr was considered a good strategy to validate the pressure dependence of the model. One can clearly see that when pressure increased, styrene formation was less significant, and at early times, the initial adduct (i1) was preferred; this pressure dependence was observed in both the experiments and the model. Overall, the model predictions agree well with the MBMS measurement in the range of T, P studied in this work. Styrene formation is overestimated by the model by ∼20−30% after 1.0 ms in the 800 K, 50 torr MBMS experiments, Figure 5d; a sensitivity analysis to address this discrepancy is presented in the next section.

4.3. Product Branching and Sensitivity Analysis. From the results of the absorbance and MBMS experiments, a kinetic model derived from the C_8H_9 PES calculated by Tokmakov and Lin has been validated. With the validated model, direct product branching ratios for the primary reaction channels can be determined. Some clarification of the relevant reaction pathways is needed to avoid confusion. In Figure 6, the major

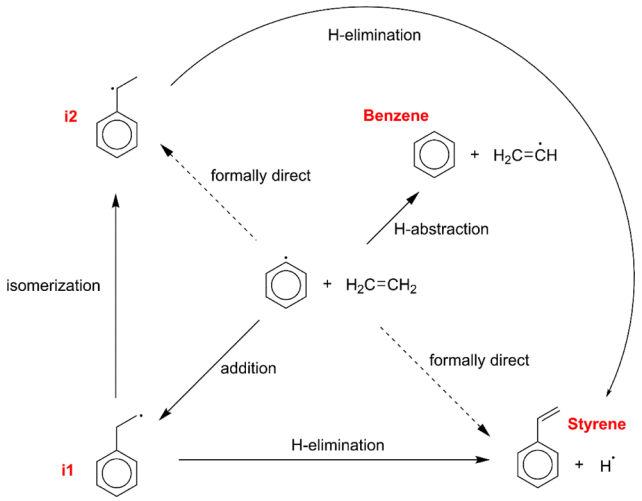

Figure 6. Important elementary steps forming major products in the C_6H_5 + C_2H_4 reaction network.

products corresponding to masses observed in the MBMS experiments are shown along with their formation pathways. The formation of i3 appears in the model with some amount at 600 K and becomes less important than that of i1 and i2 at higher temperatures. Therefore, i3 is not included in Figure 6. Solid lines represent "mechanistically direct pathways", which have one transition state connecting reactant and products, like the radical addition of C_6H_5 on C_2H_4 forming i1 and the H-abstraction reaction forming benzene + C_2H_3. Dashed lines, on the other hand, are reactions traversing more than one transition state and defined as "formally direct" pathways[81−84] including C_6H_5 + C_2H_4 (+M) → i2 (+M) and C_6H_5 + C_2H_4 (+M) → styrene + H (+M). In the $k(T, P)$ model generated from Arkane, both formally direct and mechanistically direct pathways are included. The competition between formally direct and mechanistically direct pathways consuming C_6H_5 is illustrated in Table 3 from the ROP analysis at t = 0. The product branching ratio can be related to the MBMS experiments as time-resolved product signal ratios, i.e., the signal of 104/signal of 105 and the signal of 78/signal of 105.

Table 3. Branching Ratios of Formally Direct and Mechanistically Direct Pathways Determined by ROP Analysis from C_6H_5 Consumption Predicted by the Model at Time = 0, Neglecting Side Reactions and Isomerization of the Initially Formed Products

conditions		600 K, 10 Torr	700 K, 10 Torr	800 K, 10 Torr	800 K, 50 Torr
i1	mechanistically direct pathways	93.2%	87.8%	80.2%	88.9%
benzene + C_2H_3		2.3%	4.1%	6.6%	6.4%
i2	formally direct pathways	1.9%	3.6%	5.6%	2.0%
i3		1.6%	1.8%	1.8%	1.0%
styrene + H		1.0%	2.6%	5.8%	1.6%

However, secondary reactions started to affect the product distribution after t = 0 and were more significant at longer time scales and higher temperatures. For example, thermalized i1 formed by radical addition can isomerize into i2 or eliminate H atom generating styrene. Time-resolved product signal ratios from the MBMS experiments and the model are summarized in Figures 7 and 8.

At 600 K, the formation of i1 dominates over the formation of other products, and the model predicts 93.2% of C_6H_5 reacting to form i1 through the radical addition pathway, 1.9% forming i2, and 1.6% forming i3 (for Experiment 9). As shown in Figure 5a, m/z = 105 signals are contributed predominantly by i1 at this relatively low temperature. Therefore, both the signal ratios of 104/105 and 78/105 were small, as seen in Figures 7 and 8. Since the 104 and 78 signals were small, the noise is more evident, especially on short time scales. Nevertheless, there is a decent agreement between the model and the experiments. At 600 K, secondary reactions are insignificant for t < 2 ms, so the measured products reflect the ratios of the primary reactions. Averaged from the experimental data, the short time signal ratios of 104/105 and 78/105 are 0.051 ± 0.008 and 0.082 ± 0.011. The relative yield of adducts (assuming i1 dominates and the average PICS is 10 MB), H-loss reaction (styrene + H), and H-abstraction (benzene + C_2H_3) can be quantified from MBMS experiments as

$$\text{adducts(i1 + i2 + i3): H − loss reaction: H − abstraction} = \frac{1}{\sigma_{i1}} : \frac{\frac{S_{104}}{S_{105}}}{\sigma_{\text{styrene}}} : \frac{\frac{S_{78}}{S_{105}}}{\sigma_{\text{benzene}}}$$

$$= 96.4\% \pm 1.1\% : 1.1\% \pm 0.3\% : 2.5\% \pm 0.8\%$$

The results are in good agreement with the branching predicted in Table 3, where the relative yield of adducts (i1 + i2 + i3):H-loss:H-abstraction is predicted as 96.7% : 1.0% : 2.3%.

When the temperature was increased to 700 K, the predicted branching of C_6H_5 to i2 and styrene + H increased, due to the increased importance of well-skipping reactions over adduct stabilization. Also, the predicted branching to benzene + C_2H_3 increased because higher temperature enables the reactants to cross the relatively high H-abstraction barrier. At higher temperature, secondary reactions also become faster, causing the product distribution to vary with time even at relatively short times. As shown in Figure 7b, the predicted 104/105 ratio increased by a factor of three from time 0 to 2.0 ms. Therefore, it is more challenging to determine the rate coefficient ratios from the product signals. However, given that

https://dx.doi.org/10.1021/acs.jpca.9b11543
J. Phys. Chem. A 2020, 124, 2352−2365

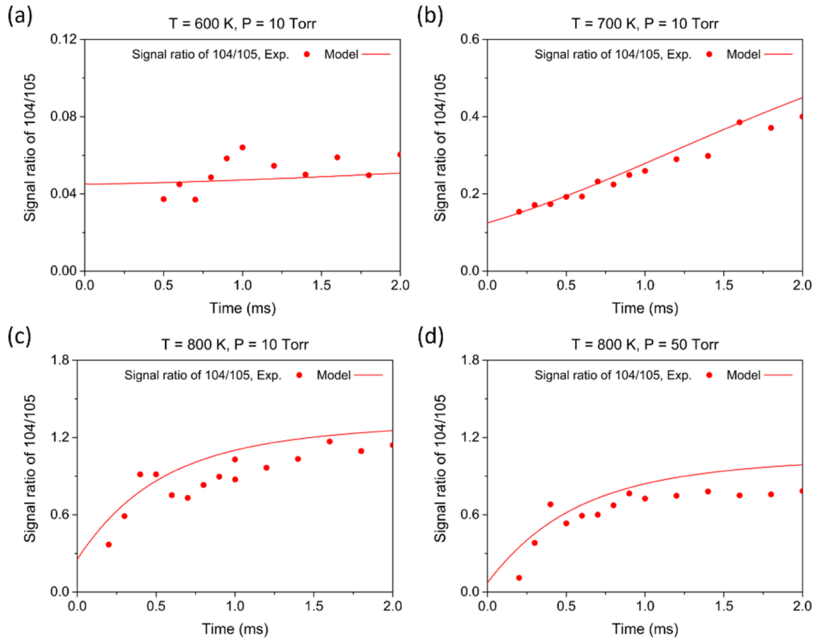

Figure 7. Signal ratio of m/z = 104−105 measured in MBMS experiments and predicted in the model, (a) 600 K, 10 Torr, (b) 700 K, 10 Torr, (c) 800 K, 10 Torr, and (d) 800 K, 50 Torr. The change in the t = 0 intercept between (c) and (d) is due to the pressure dependence of the chemically activated formation of styrene.

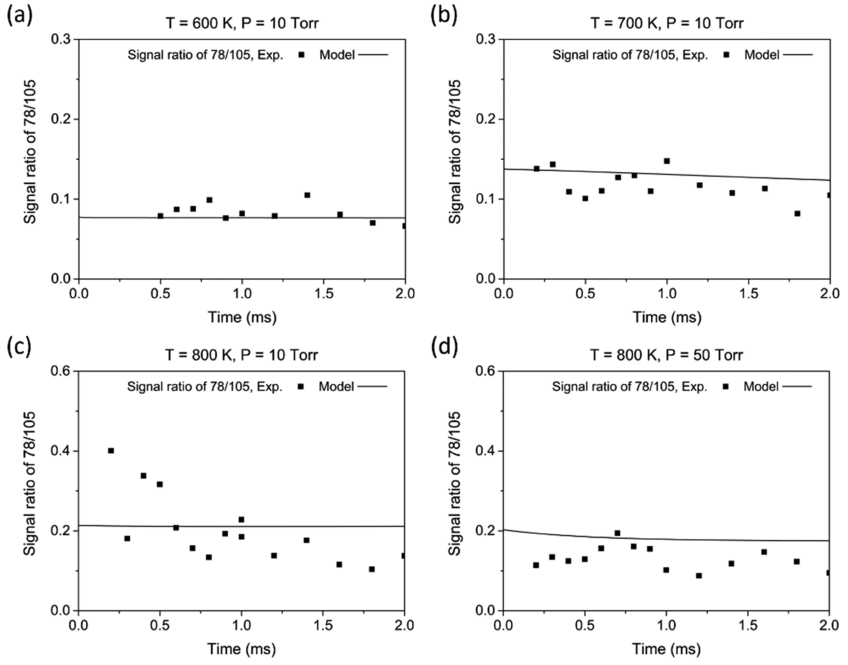

Figure 8. Signal ratio of m/z = 78−105 measured in MBMS experiments and predicted in the model, (a) 600 K, 10 Torr, (b) 700 K, 10 Torr, (c) 800 K, 10 Torr, and (d) 800 K, 50 Torr.

the time dependence of the experimental data is consistent with the model prediction in Figures 7 and 8, we conclude that the model is well validated for both direct pathways and secondary reactions.

At 700 and 800 K, the H-elimination from i1 to styrene + H plays an important role. With more i1 being converted into styrene, the 104/105 ratio increased. For the product channel of benzene + C_2H_3, the measured 78/105 signal ratio slightly decreased at 700 K between t = 0 and 2.0 ms. Although benzene + C_2H_3 formed by the mechanistically direct pathway, C_6H_5 + C_2H_4 → benzene + C_2H_3, was not affected by secondary reactions, the isomerization of i1 into i2 changed the time dependence of the 78/105 signal ratio. For each i1 isomerized into i2, the total concentration of mass 105 adducts was fixed, but the 105 signal increased because the PICS of i2 is larger than that of i1. At 800 K and 10 Torr, the predicted t = 0 branching fraction to i1 further decreased to 80.2% and secondary reactions became more important, which is supported by the fact that the 104/105 ratio increased by more than a factor of 4, and most styrene is formed by β-scission reactions from thermalized i1 and i2.

https://dx.doi.org/10.1021/acs.jpca.9b11543
J. Phys. Chem. A 2020, 124, 2352−2365

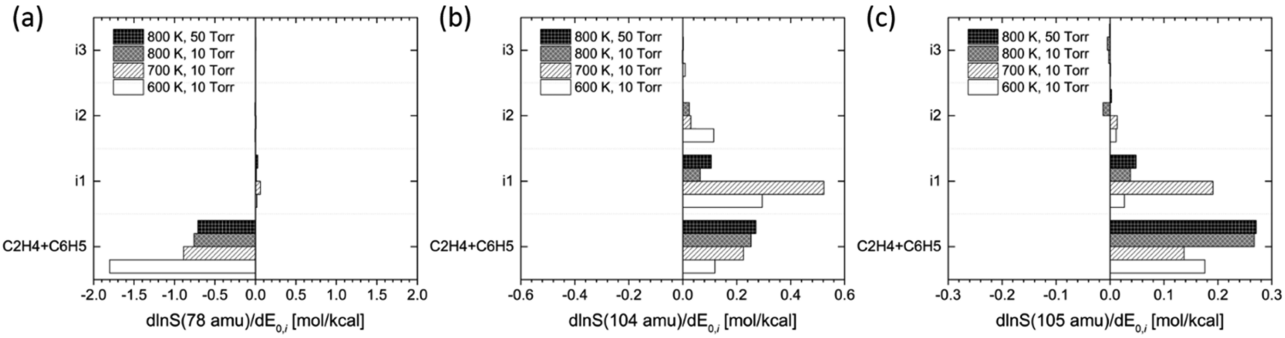

Figure 9. Sensitivity of the predicted MBMS signals to the energies E_0 of different species (combined energy of C_6H_5 + C_2H_4 is considered) in the kinetic model: (a) signals of m/z = 78, (b) signals of m/z = 104, and (c) signals of m/z = 105. Sensitivity coefficients are evaluated at 2.0 ms with the conditions of Exp. 9 (600 K, 10 Torr), 10 (700 K, 10 Torr), 12 (800 K, 10 Torr), and 15 (800 K, 50 Torr).

The change in the observed 104/105 signal ratio shown in Figure 7c,d is due to the pressure dependence of C_6H_5 + C_2H_4 → styrene + H and i1 → styrene + H. As explained by Tokmakov and Lin,[42] the effective total rate constants of the C_6H_5-addition are independent of pressure, as is the rate of the H-abstraction. The sum of branching fractions is always 100%, like the sum i1, i2, i3, styrene + H, and benzene + H in Table 3. When pressure increases, the y-axis intercept at t = 0 observed in Figure 7c,d at short times shows that the formally direct pathway of styrene + H is preferred at lower pressure over the adduct formation.

To understand how the uncertainty in quantum chemistry calculations affects the pressure-dependent kinetics in the C_8H_9 PES and the predicted MBMS signals, a sensitivity analysis was performed using Arkane to study how the kinetics on the C_8H_9 PES are affected by perturbing the zero-point energies of species (E_0) relative to C_6H_5 + C_2H_4 used in the pressure-dependent kinetics calculations. For the sensitivities to the zero-point energies of the saddle points, see the Supporting Information. Using the chain rule, the Arkane sensitivity of rate constants to E_0 was coupled with the sensitivity of species concentration to reaction rate constants and species enthalpy evaluated by RMG, and the sensitivity coefficients ($\mathrm{d} \ln S_{m/z}/\mathrm{d}E_{0,i}$) of predicted MBMS signals of m/z = 78, 104, and 105 to E_0 were evaluated. The results of $\mathrm{d} \ln S_{m/z}/\mathrm{d}E_{0,i}$ are presented in Figure 9, which shows only the sensitivity coefficients of the reactants (C_6H_5 + C_2H_4), i1, i2, and i3; for all other species on the C_8H_9 PES, the predicted signals under the studied conditions showed negligible sensitivity to varying the species E_0.

At 800 K, 50 torr, 2.0 ms, the modeled styrene signals overestimated the experimental signals by ~20−30%, as seen in Figure 5d. The sensitivity coefficients of the styrene (m/z = 104) signal to the assumed E_0 values are shown in Figure 9b. The styrene signal is sensitive to the energy of the reactants C_6H_5 + C_2H_4 and also to the energy of i1. If the zero-point energy of C_6H_5 + C_2H_4 varies by 1 kcal/mol, Figure 9b indicates a change of 30% in the m/z = 104 signal at 800 K, 50 Torr. At the G2M(RCC5)//B3LYP level of theory used in the model, an uncertainty in E_0 of about 1−2 kcal/mol is expected,[42] which is responsible for ~30−60% uncertainty in the absolute value of signals at m/z = 104. In addition to the uncertainty in E_0, there may be uncertainty due to the faster rate of side reactions such as adduct radicals reacting with the I atom at high temperatures, which compete with i1 → styrene + H and i2 → styrene + H. Some signals of m/z = 232 (C_8H_9 adduct + I atom) were observed in experiments 15 and 16. Kinetics of these side reactions are significantly uncertain, and the signals of styrene were only affected after 1.0 ms at 800 K, 50 torr; thus, the model in this work does not include these side reactions. Considering the uncertainty due to E_0 and side reactions, the difference in styrene signals between the measurement and the model can reasonably fall within the model uncertainty.

The absolute values of the sensitivity coefficients in Figure 9 indicate that product formation is only sensitive to the energies of C_6H_5, C_2H_4, i1, and i2. The species with the next highest sensitivity is i3, which has negligible values in all experimental conditions. Given the low sensitivity coefficients of the other species, the extended group additivity method, which has a 3−5 kcal/mol mean absolute error for cyclic species, is sufficient for estimating the energy and thermochemical properties of these insensitive species.[69] In summary, both the temperature and pressure dependence of the model developed from the C_8H_9 PES were validated by MBMS experiments. The full pressure-dependent mechanism is given in the Supporting Information.

5. CONCLUSIONS

The C_6H_5 + C_2H_4 reaction network was investigated experimentally with laser absorbance and MBMS experiments combined in a unique apparatus and theoretically with a pressure-dependent model developed using Tokmakov and Lin's C_8H_9 PES. The total consumption rate coefficients, $k_{\mathrm{total}}(T)$, of C_6H_5 were measured from 400 to 800 K using laser absorption at 505.3 nm and showed satisfactory agreement with the calculated values. In the previous experimental work, the rate coefficients of C_6H_5 + C_2H_4 were determined experimentally at low (297−523 K) and high (1000−1300 K) temperatures. With our new measurements performed at intermediate temperatures, the Arrhenius expression $k_{\mathrm{total}}(T) = k_{\text{R-addition}} + k_{\text{H-abstraction}} = (4.41 \times 10^5)T^{1.96} \exp(-971/T) + (9.45 \times 10^{-3})T^{4.47} \exp(-2250/T)$ has been fully verified over a wide temperature range as well as the barrier heights calculated by the G2M(RCC5)//B3LYP method.

The MBMS experiments provide direct product quantification on the C_6H_5 + C_2H_4 reaction network, which has never been reported before. Careful alignment of the photolysis laser enabled a faster rate of molecular beam sampling, allowing us to measure reaction chemistry at shorter times after the flash. Within the time scale of C_6H_5 decay, signals from adducts, H-elimination products, and H-abstraction products were observed and quantified. Predicted time profiles for the signals at m/z = 105, 104, and 78 peaks were obtained using a model

https://dx.doi.org/10.1021/acs.jpca.9b11543
J. Phys. Chem. A 2020, 124, 2352−2365

consisting of phenomenological pressure-dependent rate coefficients, $k(T, P)$, and accurate thermochemical properties both derived from the quantum chemistry calculations of Tokmakov and Lin. The experimental measurements under different T, P conditions verified the accuracy of the model. Increasing the temperature from 600 to 800 K clearly increased styrene formation, which is an important polymer precursor and significant in HACA pathways leading to PAHs. Sensitivity analysis suggested the importance of accurate C_6H_5, C_2H_4, i1, and i2 thermochemistry, which were carefully considered in the model. At higher pressures of 50 Torr, more adducts were observed relative to experiments at 10 Torr, in agreement with the pressure dependence predicted by the model.

A known disadvantage of mass spectrometry experiments is the inability to distinguish isomers; here, the validated model was used to understand the formation of two adducts with the same mass-to-charge ratio, i1 and i2. Since their total signals in the model agreed with the MBMS experiments, individual signals of i1 and i2 can be obtained from the model prediction. A ROP analysis was performed and showed that the i1 formation channel dominates the consumption of C_6H_5 at 600 K 10 Torr (93.2%) but is less important at 800 K 10 Torr (80.2%). At 600 K, the branching ratio of the H-loss channel forming styrene + H was directly measured using a high C_2H_4 concentration to minimize secondary reactions and agrees well with the model, which predicts that formation of i1 is the main contribution to the m/z = 105 signal. As pressure increases, the predicted branching to the formally direct products, i2 and styrene + H, decreases due to the higher collisional stabilization of i1. The effects of secondary reactions such as i1 isomerization and i1 H-elimination are important at high temperatures and longer times, which can be seen in the time-resolved 104/105 signal ratio. Given its complete validation by the experiment, the pressure-dependent rate coefficients developed in this work are recommended for modeling systems including the C_6H_5 + C_2H_4 reaction network.

■ ASSOCIATED CONTENT

Supporting Information

The Supporting Information is available free of charge at https://pubs.acs.org/doi/10.1021/acs.jpca.9b11543.

High-pressure-limit kinetics from the model and the additional results from the LAS and MBMS experiments are reported; pressure-dependent kinetics in Plog format (PDF)

Chemkin mechanism and species dictionary (ZIP)

Quantum calculation output files for 1-phenylethyl radical (ZIP)

Results of sensitivity analysis (XLSX)

■ AUTHOR INFORMATION

Corresponding Author

William H. Green − *Department of Chemical Engineering, Massachusetts Institute of Technology, Cambridge, Massachusetts 02139, United States;* orcid.org/0000-0003-2603-9694; Email: whgreen@mit.edu

Authors

Te-Chun Chu − *Department of Chemical Engineering, Massachusetts Institute of Technology, Cambridge, Massachusetts 02139, United States;* orcid.org/0000-0002-8475-7697

Zachary J. Buras − *Department of Chemical Engineering, Massachusetts Institute of Technology, Cambridge, Massachusetts 02139, United States;* orcid.org/0000-0001-8831-6218

Brook Eyob − *Department of Chemical Engineering, Massachusetts Institute of Technology, Cambridge, Massachusetts 02139, United States*

Mica C. Smith − *Department of Chemical Engineering, Massachusetts Institute of Technology, Cambridge, Massachusetts 02139, United States*

Mengjie Liu − *Department of Chemical Engineering, Massachusetts Institute of Technology, Cambridge, Massachusetts 02139, United States;* orcid.org/0000-0003-2414-1986

Complete contact information is available at: https://pubs.acs.org/10.1021/acs.jpca.9b11543

Notes

The authors declare no competing financial interest.

■ ACKNOWLEDGMENTS

We gratefully acknowledge Colin Grambow's help with the Molpro and Q-Chem calculations. This research was supported by SABIC. Te-Chun Chu received additional fellowship funding from the Think Global Education Trust (Taiwan).

■ REFERENCES

(1) Ehrenfreund, P. Molecules on a Space Odyssey. *Science* **1999**, *283*, 1123−1124.

(2) Zhao, L.; Kaiser, R. I.; Xu, B.; Ablikim, U.; Ahmed, M.; Joshi, D.; Veber, G.; Fischer, F. R.; Mebel, A. M. Pyrene Synthesis in Circumstellar Envelopes and Its Role in the Formation of 2d Nanostructures. *Nat. Astron.* **2018**, *2*, 413−419.

(3) Zhao, L.; Kaiser, R. I.; Xu, B.; Ablikim, U.; Ahmed, M.; Evseev, M. M.; Bashkirov, E. K.; Azyazov, V. N.; Mebel, A. M. Low-Temperature Formation of Polycyclic Aromatic Hydrocarbons in Titan's Atmosphere. *Nat. Astron.* **2018**, *2*, 973−979.

(4) Johansson, K. O.; Head-Gordon, M. P.; Schrader, P. E.; Wilson, K. R.; Michelsen, H. A. Resonance-Stabilized Hydrocarbon-Radical Chain Reactions May Explain Soot Inception and Growth. *Science* **2018**, *361*, 997−1000.

(5) Barak, S.; Rahman, R. K.; Neupane, S.; Ninnemann, E.; Arafin, F.; Laich, A.; Terracciano, A. C.; Vasu, S. S. Measuring the Effectiveness of High-Performance Co-Optima Biofuels on Suppressing Soot Formation at High Temperature. *Proc. Natl. Acad. Sci. U.S.A.* **2020**, *117*, 3451−3460.

(6) Dandajeh, H. A.; Ladommatos, N.; Hellier, P.; Eveleigh, A. Influence of Carbon Number of C1−C7 Hydrocarbons on Pah Formation. *Fuel* **2018**, *228*, 140−151.

(7) Liu, P.; Li, Z.; Roberts, W. L. The Growth of Pahs and Soot in the Post-Flame Region. *Proc. Combust. Inst.* **2019**, *37*, 977−984.

(8) Park, S.; Wang, Y.; Chung, S. H.; Sarathy, S. M. Compositional Effects on Pah and Soot Formation in Counterflow Diffusion Flames of Gasoline Surrogate Fuels. *Combust. Flame* **2017**, *178*, 46−60.

(9) Veshkini, A.; Eaves, N. A.; Dworkin, S. B.; Thomson, M. J. Application of Pah-Condensation Reversibility in Modeling Soot Growth in Laminar Premixed and Nonpremixed Flames. *Combust. Flame* **2016**, *167*, 335−352.

(10) Kholghy, M. R.; Veshkini, A.; Thomson, M. J. The Core−Shell Internal Nanostructure of Soot − a Criterion to Model Soot Maturity. *Carbon* **2016**, *100*, 508−536.

(11) Finlayson-Pitts, B. J.; Pitts, J. N. Tropospheric Air Pollution: Ozone, Airborne Toxics, Polycyclic Aromatic Hydrocarbons, and Particles. *Science* **1997**, *276*, 1045−1051.

(12) Johansson, K. O.; Zádor, J.; Elvati, P.; Campbell, M. F.; Schrader, P. E.; Richards-Henderson, N. K.; Wilson, K. R.; Violi, A.; Michelsen, H. A. Critical Assessment of Photoionization Efficiency Measurements for Characterization of Soot-Precursor Species. *J. Phys. Chem. A* **2017**, *121*, 4475−4485.
(13) Ricks, A. M.; Gary, E. D.; Michael, A. D. The Infrared Spectrum of Protonated Naphthalene and Its Relevance for the Unidentified Infrared Bands. *Astrophys. J.* **2009**, *702*, 301.
(14) Tielens, A. G. G. M. Interstellar Polycyclic Aromatic Hydrocarbon Molecules. *Annu. Rev. Astron. Astrophys.* **2008**, *46*, 289−337.
(15) Tielens, A. G. G. M. *The Physics and Chemistry of the Interstellar Medium*; Cambridge University Press: Cambridge, 2005.
(16) Peeters, E.; Mattioda, A. L.; Hudgins, D. M.; Allamandola, L. J. Polycyclic Aromatic Hydrocarbon Emission in the 15-21 Micron Region. *Astrophys. J. Lett.* **2004**, *617*, L65−L68.
(17) Duley, W. W. Polycyclic Aromatic Hydrocarbons, Carbon Nanoparticles and the Diffuse Interstellar Bands. *Faraday Discuss.* **2006**, *133*, 415−425.
(18) Salama, F.; Bakes, E. L.; Allamandola, L. J.; Tielens, A. G. Assessment of the Polycyclic Aromatic Hydrocarbon-Diffuse Interstellar Band Proposal. *Astrophys. J.* **1996**, *458*, 621−636.
(19) Ehrenfreund, P.; Sephton, M. A. Carbon Molecules in Space: From Astrochemistry to Astrobiology. *Faraday Discuss.* **2006**, *133*, 277−288.
(20) Ehrenfreund, P.; Charnley, S. B. Organic Molecules in the Interstellar Medium, Comets, and Meteorites: A Voyage from Dark Clouds to the Early Earth. *Annu. Rev. Astron. Astrophys.* **2000**, *38*, 427−483.
(21) Dwek, E.; Arendt, R. G.; Fixsen, D. J.; Sodroski, T. J.; Odegard, N.; Weiland, J. L.; Reach, W. T.; Hauser, M. G.; Kelsall, T.; Moseley, S. H.; et al. Detection and Characterization of Cold Interstellar Dust and Polycyclic Aromatic Hydrocarbon Emission, from Cobe Observations. *Astrophys. J.* **1997**, *475*, 565−579.
(22) Di, Q.; Dai, L.; Wang, Y. Association of Short-Term Exposure to Air Pollution with Mortality in Older Adults. *JAMA* **2017**, *318*, 2446−2456.
(23) Shindell, D.; Kuylenstierna, J. C. I.; Vignati, E.; van Dingenen, R.; Amann, M.; Klimont, Z.; Anenberg, S. C.; Muller, N.; Janssens-Maenhout, G.; Raes, F.; et al. Simultaneously Mitigating near-Term Climate Change and Improving Human Health and Food Security. *Science* **2012**, *335*, 183−189.
(24) Mebel, A. M.; Georgievskii, Y.; Jasper, A. W.; Klippenstein, S. J. Temperature- and Pressure-Dependent Rate Coefficients for the Haca Pathways from Benzene to Naphthalene. *Proc. Combust. Inst.* **2017**, *36*, 919−926.
(25) Richter, H.; Howard, J. B. Formation of Polycyclic Aromatic Hydrocarbons and Their Growth to Soot—a Review of Chemical Reaction Pathways. *Prog. Energy Combust. Sci.* **2000**, *26*, 565−608.
(26) Frenklach, M.; Wang, H. Detailed Modeling of Soot Particle Nucleation and Growth. *Symp. (Int.) Combust.* **1991**, *23*, 1559−1566.
(27) Frenklach, M.; Clary, D. W.; Gardiner, W. C.; Stein, S. E. Detailed Kinetic Modeling of Soot Formation in Shock-Tube Pyrolysis of Acetylene. *Symp. (Int.) Combust.* **1985**, *20*, 887−901.
(28) Orr, S. T. M.; Ripp, S. L.; Ballard, T. E.; Henderson, J. L.; Scott, D. O.; Obach, R. S.; Sun, H.; Kalgutkar, A. S. Mechanism-Based Inactivation (Mbi) of Cytochrome P450 Enzymes: Structure−Activity Relationships and Discovery Strategies to Mitigate Drug−Drug Interaction Risks. *J. Med. Chem.* **2012**, *55*, 4896−4933.
(29) Justo, G. Z.; Livotto, P. R.; Durán, N. Chemical and Photochemical Generated Carbon-Centered Radical Intermediate and Its Reaction with Desoxyribonucleic Acid. *Free Radical Biol. Med.* **1995**, *19*, 431−440.
(30) Leite, L. C. C.; Augusto, O. DNA Alterations Induced by the Carbon-Centered Radical Derived from the Oxidation of 2-Phenylethylhydrazine. *Arch. Biochem. Biophys.* **1989**, *270*, 560−572.
(31) Ortiz de Montellano, P. R.; Watanabe, M. D. Free Radical Pathways in the in Vitro Hepatic Metabolism of Phenelzine. *Mol. Pharm.* **1987**, *31*, 213−219.
(32) Skene, W. G.; Scaiano, J. C.; Yap, G. P. A. An Improved Mimetic Compound for Styrene "Living" Free Radical Polymerization. An Initiator Containing the "Penultimate" Unit. *Macromolecules* **2000**, *33*, 3536−3542.
(33) Bevington, J. C.; Cywar, D. A.; Huckerby, T. N.; Senogles, E.; Tirrell, D. A. Reactivities of Monomers Towards the 1-Phenylethyl Radical. *Eur. Polym. J.* **1990**, *26*, 41−46.
(34) Cywar, D. A.; Tirrell, D. A. Model Copolymerization Reactions. Determination of the Relative Rates of Addition of Styrene and Acrylonitrile to the 1-Phenylethyl Radical. *Macromolecules* **1986**, *19*, 2908−2911.
(35) Ito, K.; Omi, M.; Ito, T. Kinetics of Radical Polymerization with Primary Radical Termination. *Polym. J.* **1982**, *14*, 115−120.
(36) Fahr, A.; Stein, S. E. Reactions of Vinyl and Phenyl Radicals with Ethyne, Ethene and Benzene. *Symp. (Int.) Combust.* **1989**, *22*, 1023−1029.
(37) Fahr, A.; Gary Mallard, W.; Stein, S. E. Reactions of Phenyl Radicals with Ethene, Ethyne, and Benzene. *Symp. (Int.) Combust.* **1988**, *21*, 825−831.
(38) Yu, T.; Lin, M. C. Kinetics of the Phenyl Radical Reaction with Ethylene: An Rrkm Theoretical Analysis of Low and High Temperature Data. *Combust. Flame* **1995**, *100*, 169−176.
(39) Yu, T.; Lin, M. C. Kinetics of Phenyl Radical Reactions Studied by the Cavity-Ring-Down Method. *J. Am. Chem. Soc.* **1993**, *115*, 4371−4372.
(40) Zhang, F.; Gu, X.; Guo, Y.; Kaiser, R. I. Reaction Dynamics on the Formation of Styrene: A Crossed Molecular Beam Study of the Reaction of Phenyl Radicals with Ethylene. *J. Org. Chem.* **2007**, *72*, 7597−7604.
(41) Mebel, A. M.; Morokuma, K.; Lin, M. C. Modification of the Gaussian-2 Theoretical Model: The Use of Coupled-Cluster Energies, Density-Functional Geometries, and Frequencies. *J. Chem. Phys.* **1995**, *103*, 7414−7421.
(42) Tokmakov, I. V.; Lin, M. C. Combined Quantum Chemical/Rrkm-Me Computational Study of the Phenyl + Ethylene, Vinyl + Benzene, and H + Styrene Reactions. *J. Phys. Chem. A* **2004**, *108*, 9697−9714.
(43) Buras, Z. J.; Elsamra, R. M.; Jalan, A.; Middaugh, J. E.; Green, W. H. Direct Kinetic Measurements of Reactions between the Simplest Criegee Intermediate Ch2oo and Alkenes. *J. Phys. Chem. A* **2014**, *118*, 1997−2006.
(44) Buras, Z. J.; Dames, E. E.; Merchant, S. S.; Liu, G.; Elsamra, R. M. I.; Green, W. H. Kinetics and Products of Vinyl + 1,3-Butadiene, a Potential Route to Benzene. *J. Phys. Chem. A* **2015**, *119*, 7325−7338.
(45) Middaugh, J. E.; Buras, Z. J.; Matrat, M.; Chu, T.-C.; Kim, Y.-S.; Alecu, I. M.; Vasiliou, A. K.; Goldsmith, C. F.; Green, W. H. A Combined Photoionization Time-of-Flight Mass Spectrometry and Laser Absorption Spectrometry Flash Photolysis Apparatus for Simultaneous Determination of Reaction Rates and Product Branching. *Rev. Sci. Instrum.* **2018**, *89*, 74102.
(46) Buras, Z. J.; Chu, T. C.; Jamal, A.; Yee, N. W.; Middaugh, J. E.; Green, W. H. Phenyl Radical + Propene: A Prototypical Reaction Surface for Aromatic-Catalyzed 1,2-Hydrogen-Migration and Subsequent Resonance-Stabilized Radical Formation. *Phys. Chem. Chem. Phys.* **2018**, *20*, 13191−13214.
(47) Tonokura, K.; Norikane, Y.; Koshi, M.; Nakano, Y.; Nakamichi, S.; Goto, M.; Hashimoto, S.; Kawasaki, M.; Sulbaek Andersen, M. P.; Hurley, M. D.; et al. Cavity Ring-Down Study of the Visible Absorption Spectrum of the Phenyl Radical and Kinetics of Its Reactions with Cl, Br, Cl2, and O2. *J. Phys. Chem. A* **2002**, *106*, 5908−5917.
(48) Hunziker, H. E.; Kneppe, H.; McLean, A. D.; Siegbahn, P.; Wendt, H. R. Visible Electronic Absorption Spectrum of Vinyl Radical. *Can. J. Chem.* **1983**, *61*, 993−995.
(49) Kislov, V. V.; Singh, R. I.; Edwards, D. E.; Mebel, A. M.; Frenklach, M. Rate Coefficients and Product Branching Ratios for the Oxidation of Phenyl and Naphthyl Radicals: A Theoretical Rrkm-Me Study. *Proc. Combust. Inst.* **2015**, *35*, 1861−1869.

https://dx.doi.org/10.1021/acs.jpca.9b11543
J. Phys. Chem. A 2020, 124, 2352−2365

(50) Zhang, F.; Nicolle, A.; Xing, L.; Klippenstein, S. J. Recombination of Aromatic Radicals with Molecular Oxygen. *Proc. Combust. Inst.* **2017**, *36*, 169−177.
(51) Allen, J. W.; Goldsmith, C. F.; Green, W. H. Automatic Estimation of Pressure-Dependent Rate Coefficients. *Phys. Chem. Chem. Phys.* **2012**, *14*, 1131−1155.
(52) Gao, C. W.; Allen, J. W.; Green, W. H.; West, R. H. Reaction Mechanism Generator: Automatic Construction of Chemical Kinetic Mechanisms. *Comput. Phys. Commun.* **2016**, *203*, 212−225.
(53) Joback, K. G.; Reid, R. C. Estimation of Pure-Component Properties from Group-Contributions. *Chem. Eng. Commun.* **1987**, *57*, 233−243.
(54) Mebel, A. M.; Georgievskii, Y.; Jasper, A. W.; Klippenstein, S. J. Pressure-Dependent Rate Constants for Pah Growth: Formation of Indene and Its Conversion to Naphthalene. *Faraday Discuss.* **2016**, *195*, 637−670.
(55) Jasper, A. W.; Oana, C. M.; Miller, J. A. "Third-Body" Collision Efficiencies for Combustion Modeling: Hydrocarbons in Atomic and Diatomic Baths. *Proc. Combust. Inst.* **2015**, *35*, 197−204.
(56) Narayanaswamy, K.; Blanquart, G.; Pitsch, H. A Consistent Chemical Mechanism for Oxidation of Substituted Aromatic Species. *Combust. Flame* **2010**, *157*, 1879−1898.
(57) Werner, H. J.; Knowles, P. J.; Knizia, G.; Manby, F. R.; Schütz, M. Molpro: A General-Purpose Quantum Chemistry Program Package. *WIREs Comput. Mol. Sci.* **2012**, *2*, 242−253.
(58) Knowles, P. J.; Hampel, C.; Werner, H. J. Coupled Cluster Theory for High Spin Open Shell Reference Wavefunctions. *J. Chem. Phys.* **1993**, *99*, 5219−5227.
(59) Knowles, P. J.; Werner, H. J. Internally Contracted Multi-configuration Reference Configuration Interaction Calculations for Excited States. *Theor. Chim. Acta* **1992**, *84*, 95−103.
(60) Knowles, P. J.; Andrews, J. S.; Amos, R. D.; Handy, N. C.; Pople, J. A. Restricted Møller–Plesset Theory for Open Shell Molecules. *Chem. Phys. Lett.* **1991**, *186*, 130−136.
(61) Amos, R. D.; Andrews, J. S.; Handy, N. C.; Knowles, P. J. Open Shell Møller–Plesset Perturbation Theory. *Chem. Phys. Lett.* **1991**, *185*, 256−264.
(62) Knowles, P. J.; Handy, N. C. A Determinant Based Full Configuration Interaction Program. *Comput. Phys. Commun.* **1989**, *54*, 75−83.
(63) Werner, H. J.; Knowles, P. J. An Efficient Internally Contracted Multiconfiguration Reference Ci Method. *J. Chem. Phys.* **1988**, *89*, 5803−5814.
(64) Knowles, P. J.; Werner, H. J. An Efficient Method for the Evaluation of Coupling Coefficients in Configuration Interaction Calculations. *Chem. Phys. Lett.* **1988**, *145*, 514−522.
(65) Werner, H. J.; Knowles, P. J. A Second Order Mcscf Method with Optimum Convergence. *J. Chem. Phys.* **1985**, *82*, 5053.
(66) Knowles, P. J.; Werner, H. J. An Efficient Second Order Mcscf Method for Long Configuration Expansions. *Chem. Phys. Lett.* **1985**, *115*, 259−267.
(67) Knowles, P. J.; Handy, N. C. A New Determinant-Based Full Configuration Interaction Method. *Chem. Phys. Lett.* **1984**, *111*, 315−321.
(68) Shao, Y.; Gan, Z.; Epifanovsky, E.; Gilbert, A. T. B.; Wormit, M.; Kussmann, J.; Lange, A. W.; Behn, A.; Deng, J.; Feng, X.; et al. Advances in Molecular Quantum Chemistry Contained in the Q-Chem 4 Program Package. *Mol. Phys.* **2015**, *113*, 184−215.
(69) Han, K.; Jamal, A.; Grambow, C. A.; Buras, Z. J.; Green, W. H. An Extended Group Additivity Method for Polycyclic Thermochemistry Estimation. *Int. J. Chem. Kinet.* **2018**, *50*, 294−303.
(70) *Chemical Workbench 4.1.18493*; Kintech Lab: Moscow, Russia, 2016.
(71) Cool, T. A.; Wang, J.; Nakajima, K.; Taatjes, C. A.; McLlroy, A. Photoionization Cross Sections for Reaction Intermediates in Hydrocarbon Combustion. *Int. J. Mass Spectrom.* **2005**, *247*, 18−27.
(72) Zhou, Z.; Xie, M.; Wang, Z.; Qi, F. Determination of Absolute Photoionization Cross-Sections of Aromatics and Aromatic Derivatives. *Rapid Commun. Mass Spectrom.* **2009**, *23*, 3994−4002.
(73) Xu, H.; Pratt, S. T. Photoionization Cross Section of the Propargyl Radical and Some General Ideas for Estimating Radical Cross Sections. *J. Phys. Chem. A* **2013**, *117*, 9331−9342.
(74) Dyakov, Y. A.; Hsu, W. H.; Ni, C. K.; Tsai, W. C.; Hu, W. P. Photodissociation Dynamics of Benzyl Alcohol at 193 Nm. *J. Chem. Phys.* **2012**, *137*, No. 064314.
(75) Baeza-Romero, M. T.; Blitz, M. A.; Goddard, A.; Seakins, P. W. Time-of-Flight Mass Spectrometry for Time-Resolved Measurements: Some Developments and Applications. *Int. J. Chem. Kinet.* **2012**, *44*, 532−545.
(76) Ha, T.-K.; He, Y.; Pochert, J.; Quack, M.; Ranz, R.; Seyfang, G.; Thanopoulos, I. Absolute Integrated Band Strength and Magnetic Dipole Transition Moments in the 2p3/2 → 2p1/2 Fine Structure (with Hyperfine Structure) Transition of the Iodine Atom: Experiment and Theory. *Ber. Bunsen-Ges. Phys. Chem.* **1995**, *99*, 384−392.
(77) Ismail, H.; Abel, P. R.; Green, W. H.; Fahr, A.; Jusinski, L. E.; Knepp, A. M.; Zádor, J.; Meloni, G.; Selby, T. M.; Osborn, D. L.; et al. Temperature-Dependent Kinetics of the Vinyl Radical (C2h3) Self-Reaction. *J. Phys. Chem. A* **2009**, *113*, 1278−1286.
(78) Yaws' Critical Property Data for Chemical Engineers and Chemists, 2012. http://app.knovel.com/hotlink/toc/id:kpYCPDCECD/yaws-critical-property/yaws-critical-property.
(79) Osborn, D. L.; Zou, P.; Johnsen, H.; Hayden, C. C.; Taatjes, C. A.; Knyazev, V. D.; North, S. W.; Peterka, D. S.; Ahmed, M.; Leone, S. R. The Multiplexed Chemical Kinetic Photoionization Mass Spectrometer: A New Approach to Isomer-Resolved Chemical Kinetics. *Rev. Sci. Instrum.* **2008**, *79*, No. 104103.
(80) Wong, B. M.; Matheu, D. M.; Green, W. H. Temperature and Molecular Size Dependence of the High-Pressure Limit. *J. Phys. Chem. A* **2003**, *107*, 6206−6211.
(81) Zádor, J.; Taatjes, C. A.; Fernandes, R. X. Kinetics of Elementary Reactions in Low-Temperature Autoignition Chemistry. *Prog. Energy Combust. Sci.* **2011**, *37*, 371−421.
(82) Knepp, A. M.; Meloni, G.; Jusinski, L. E.; Taatjes, C. A.; Cavallotti, C.; Klippenstein, S. J. Theory, Measurements, and Modeling of Oh and Ho2 Formation in the Reaction of Cyclohexyl Radicals with O2. *Phys. Chem. Chem. Phys.* **2007**, *9*, 4315−4331.
(83) Estupiñán, E. G.; Smith, J. D.; Tezaki, A.; Klippenstein, S. J.; Taatjes, C. A. Measurements and Modeling of Do2 Formation in the Reactions of C2d5 and C3d7 Radicals with O2. *J. Phys. Chem. A* **2007**, *111*, 4015−4030.
(84) DeSain, J. D.; Klippenstein, S. J.; Miller, J. A.; Taatjes, C. A. Measurements, Theory, and Modeling of Oh Formation in Ethyl + O2 and Propyl + O2 Reactions. *J. Phys. Chem. A* **2003**, *107*, 4415−4427.

https://dx.doi.org/10.1021/acs.jpca.9b11543
J. Phys. Chem. A 2020, 124, 2352−2365